Synthetic superstructures showing polymorphism, coherent responsiveness, and parallel reactions in phase separation

Priyadarshi Ranjan[1]*, Moussa Diame Faye Diouf[2], Aswin Asaithambi[1], Iyyappa Rajan Panneerselvam [3], Yan Wang[4], Liberato Manna[3], Mauro Gemmi[2], Ilka Kriegel [1,5]*

[1]Functional Nanosystems, Istituto Italiano di Tecnologia; Genova, 16163, Italy
[2]Electron Crystallography, Center for Materials Interfaces, Istituto Italiano di Tecnologia; Pontedera, 56025, Italy
[3]Nanochemistry, Istituto Italiano di Tecnologia; Genova, 16163, Italy
[4]Department of Mechanical Engineering, University of Nevada; Reno, 89557, USA
[5]Dipartimento di Scienza Applicata e Tecnologie (DISAT), Politecnico di Torino; Torino, 10129, Italy

*Corresponding author. Email: priyadarshi.ranjan@iit.it & ilka.kriegel@iit.it

KEYWORDS: Supramolecular Polymers, Chiral, Curved structures, Phase Separation, Droplets, Hierarchical assembly, Azobenzene, Photomechanics, Responsiveness

Abstract: Understanding and mimicking the processes of life has been an endeavour for generations of scientists across all the fields of science and technology. Artificially designing the complexity of living cells from purely synthetic materials poses a significant challenge due to their complex bottom-up assembly. We show that a solvothermal reaction of pre-formed sodium coordinated pyrene and porphyrin based supramolecular structures with azobenzene supramolecules in a one-pot reaction results in an array of superstructures with controlled morphology, featuring curved surfaces and extrinsic chirality. They respond as a single unit to external triggers, such as light, exhibiting transformations to macro-scale extrinsic chirality, as well as bursting and folding behaviours. Finally, we show the growth of two different types of superstructures in parallel by exploiting liquid-liquid phase separation.

Superstructures (co-assemblies) are complex architectures formed from individual components through a hierarchical self-assembly.(*1*) Each component added during the formation of superstructures is a carrier of specific information. Any change in the chemical's properties (also introduced by external stimuli before and/or after the interaction) will impact the entire superstructures.(*2*) There is a need to develop simple methods, able to expose the effect of an individual component on the superstructure formation process, despite the high level of complexity.(*3–5*) A model system, which allows us to trigger the behavior of individual components in multicomponent mixtures, will enable us to understand the process of artificial superstructure formation.(*4*) Precise control over superstructure formation is expected to open new areas of synthetic chemistry, understanding of prebiotic chemistry, and facilitating the creation of more sophisticated materials, where the composition, structure, and functionality can be designed for a specific application.(*3*, *6–8*) Finally, synthetic chemistry has long aspired to perform multicomponent reactions in phase-separated compartments to form multiple co-assemblies at the same time that operate separately but function synergistically. The precise spatiotemporal organization of superstructures is often manifested by phase transitions,(*9*) where reactions occur in parallel exploiting information transfer, while maintaining high dynamics.(*3*, *6*, *7*)

Rationally designed synthetic superstructures can also provide insight into the progressive emergence of complex life.(*6*, *10*, *11*) Complexity observed in natural processes employs phase-separated co-assemblies for parallel reactions to enhance efficiency, sophistication and to reduce noise.(*6*, *12*, *13*) Phase separated co-assemblies are membrane-less assemblies represented as droplets in a matrix (such as the nucleolus in the cytoplasm).(14) The membrane-less assemblies often undergo multiphase structuring depending upon their relative surface tensions (γ_{ij}). (*16*, *17*) Often, multivalent protein-protein (and protein-RNA) interactions are an important driving force for multiphase structuring of the droplets.(*18*)

During physiological conditions soluble molecules form the liquid phase, whereas under pathological conditions they develop into solid-like condensed states due to stronger interactions.(16) Further, droplets' interfaces have the potential to speed up protein aggregation, and the interfacial exchange dynamics of biomolecular droplets are highly responsive to interactions with clients.(*19*, *20*) The synthetic reconstruction of cellular architecture is becoming increasingly pertinent, focusing to date on the crowding effect and phase separation caused by small molecules.(21–24) Controlling reaction kinetics within individual liquid-liquid phase separation (LLPS) layers is still unexplored for synthetic chemists.(*22*, *23*, *26*, *27*)

Here, we present a one-pot-reaction method to form polymorphs of superstructures as model systems to simulate naturally occurring co-assembly. We use pyrene-based multidentate ligands together with supramolecular photoisomers constituting azobenzene derivatives in addition to sodium hydroxide [1M] in a one-pot solvothermal reaction. We employ supramolecules of sodium coordinated 4,4',4",4"'-(Pyrene-1,3,6,8-tetrayl)tetrabenzoic acid (in the following Na-PyrTBA) as one of the components in the synthesis of the superstructures. Pyrene-based ligands are often used for synthesis of porous and versatile metal-organic frameworks (MOFs) and covalent-organic frameworks (COFs).(*28*, *29*) Very few stable sodium based MOFs have been reported, showing high porosity and used for gas storage.(*30*) As the azobenzene unit, we chose a pair of positional azobenzenes and their geometrical counterparts, namely 4-(4-hydroxyphenylazo)benzoic acid and 2-(4-hydroxy-phenylazo)-benzoic acid. Azobenzene moieties and their derivatives are well known for their ability to isomerize upon exposure to light.(*31*) The geometric *Z*- and *E*- isomers vary in shape and polarity.(*32*) All the derivatives in the set have carboxylic and hydroxy end groups. Deprotonation of the carboxylic end group leads to intermolecular hydrogen bonding and the formation of supramolecules (in the following *E/Z*-4HPBA and *E/Z*-2HPBA). These supramolecules have a similar chemical functionality as that of Na-PyrTBA, thereby enabling multivalent interactions, leading to the formation of superstructure polymorphs.

In the following, we will show superstructure formation with varying morphology as a result of the solvothermal reaction of Na-pyrene-based supramolecules with azobenzene-based supramolecules and Zirconium (Zr). By passing on exact chemical information of a particular azobenzene derivative, the nature of the polymorphic superstructure is determined. The induced photomechanical response of the azobenzene derivatives (*33*) upon photoisomerization evokes coherent responsiveness of the superstructure with light as trigger. The exhibited responsiveness elucidates the guide nature of the azobenzene supramolecules in the bigger superstructure. Previous studies of responsiveness at the molecular level were limited to the controlled opening and closing of pores, disintegration of a closed structure upon light response and the periodic bending motion of the photoactive framework at a local scale.(*34*, *35*) Here instead we show transformations that induce chirality, as well as bursting and folding behaviours. The resultant supramolecules are formed through transitions from liquid phase to solid phase, whilst photoisomeric supramolecules govern the assembly process bringing forth the polymorphism.

In the following, we discuss our results in the following on two levels differentiated by the type and quantity of components in the multicomponent reaction mixture. The initial level investigates the polymorphism of Na-pyrene-based MOF superstructures within a dispersion, prompted by a set of supramolecular photoisomers resulting in multiphase structuring. This is followed by examining their coherent responsiveness to various wavelengths of light. At the next level, the complexity of the system is increased by introducing an additional Na-porphyrin-based supramolecule, leading to phase separation driven by this added complexity.(*36*) The supramolecular photoisomers regulate the diversity within the different phases, resulting in two distinctly separate sets of superstructures forming in each phase, thereby illustrating parallel reactions.

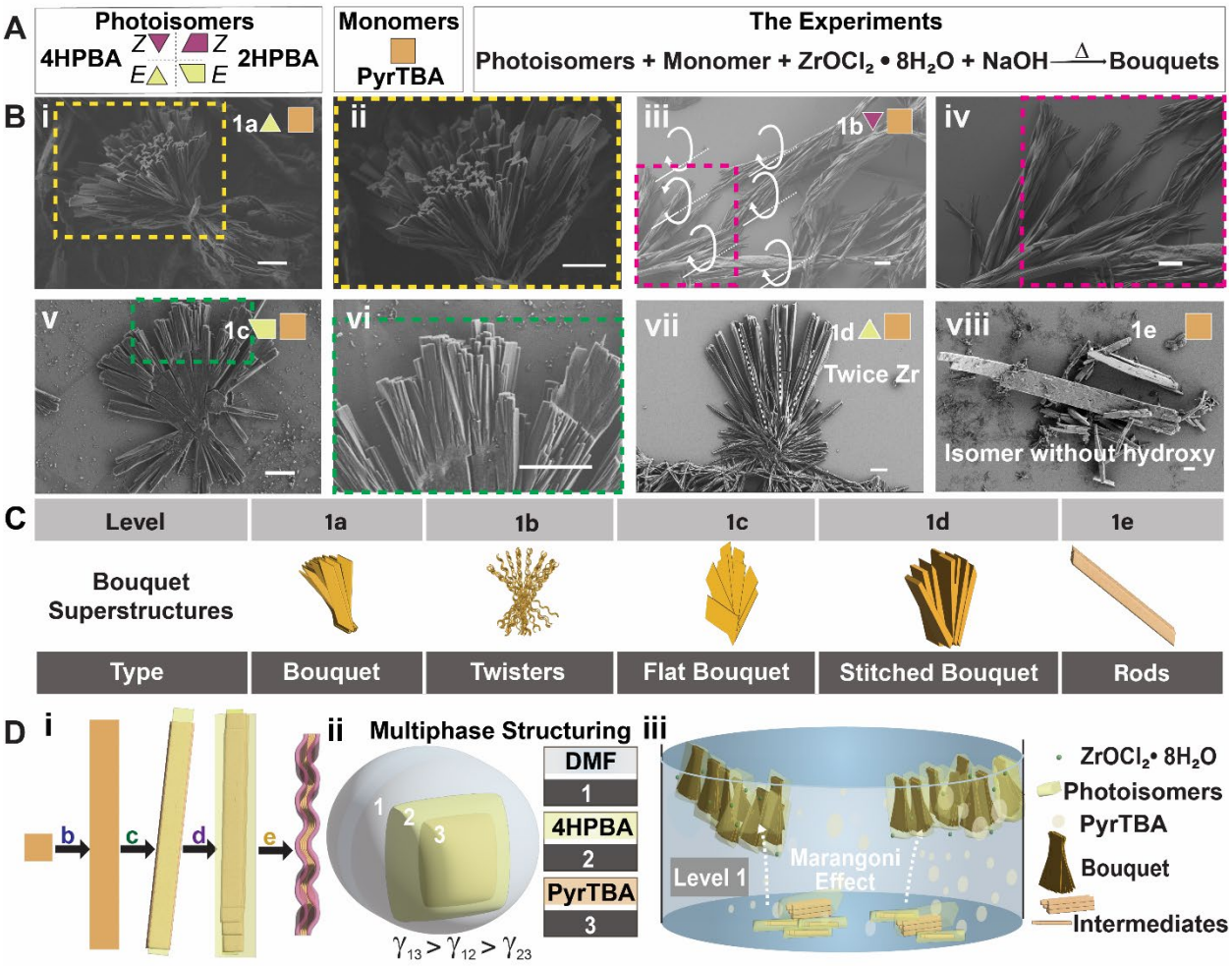

Fig. 1. Formation of Bouquet Superstructures in dispersion. (**A**) A set of solvothermal reactions of monomer PyrTBA directed by a set of supramolecular photoisomer results into bouquet superstructures. (**B**) SEM images of (i) & (ii) bouquets (1a), (iii) & (iv) twisted bouquets (1b), v & vi flat bouquets (1c), vii stitched bouquets (1d), and rods (1e). Scale bar = 2 µm. (**C**) Schematic illustration of the set of bouquet superstructures evolved in various conditions. (**D**) (i) Illustration of PyrTBA superstructures with *E*-4HPBA. (ii) The relative surface tensions among the solvent (DMF), 4HPBA and Na-PyrTBA interfaces (γ_{ij}) dictate the droplet architecture resulting in multiphase structuring. (iii) Illustration of the formation of superstructures elicited by Marangoni effect.

Level 1 Complexity: A set of Bouquet Superstructures in dispersions.

In Fig. 1A, we show a scheme of the solvothermal reaction of supramolecular PyrTBA with supramolecular photoisomers (*E/Z*-4HPBA and *E/Z*-2HPBA) in the presence of sodium hydroxide [1M] and Zr salt. Typically, the monomer of PyrTBA (i.e., 4,4',4",4"'-(Pyrene-1,3,6,8-tetrayl)tetrabenzoic acid) is used as a ligand together with Zr salt in the presence of benzoic acid as a modulator to synthesize highly robust mesoporous MOFs in basic environment.(*37*) We designed the experiments to make a MOF with mixed metal clusters and multiple ligands. We planned to use sodium to coordinate with multiple ligands and Zr to offer rigidity. Generally, during the synthesis of MOFs, the whole ligand mixture is sonicated, and a base is added during the sonication process to fully dissolve in the solvent and then added to already modulated Zr dispersions.(*37*, *38*) With the initial intention to coordinate supramolecular photoisomers and the PyrTBA to both Na and Zr, we altered the procedure (for details of the reaction procedure, please see Supplementary Information). We pre-synthesized the supramolecular photoisomers and used comparatively lesser amount of Zr salt than used typically for MOF syntheses. For this purpose, we had chosen similar chemically functionalized

monomers and photoisomers. We separately sonicated the monomer of PyrTBA with sodium hydroxide [1M] to form a supramolecule as a building block, as well as the azobenzene derivatives to form supramolecular photoisomers. The different structures and the optical properties obtained from the supramolecular photoisomers after sonicating with sodium hydroxide [1M] are discussed in Fig. S1. Supramolecular Na-PyrTBA itself forms planks, as shown in Fig. S2. Subsequently, the mixture of the supramolecular photoisomer, i.e. *E/Z*-4HPBA or *E/Z*-2HPBA with the Na-PyrTBA (at a molar ratio of 4:1PyrTBA to photoisomer) was then added to the pre-heated Zr dispersion and put in a reactor for the solvothermal reaction. The reaction was left to cool slowly for two days to promote crystallization. SEM analysis of the crystals reveals that superstructures are formed, whose morphology is controlled by the respective supramolecular photoisomers (Fig. 1A). The SEM images in Fig. 1B and sketches in Fig. 1C show that bouquet-type structures (1a), twisters (1b), and flat bouquets (1c), are formed depending on the supramolecular photoisomers chosen (Fig. 1B(i-vi)). Superstructure 1a, formed with *E*-4HPBA as photoisomer, consists of planks that are protruding and opening from a common head as shown in Fig. 1B(i-ii). 3D Electron Diffraction (3DED) analysis reveals that 1a crystallizes in the monoclinic crystal system with a space group of $P2_1/c$ (Table S1).(*39*)

To understand better the assembly process and the role of each component on the superstructure formation, we separated each step of the reaction, starting with the PyrTBA supramolecule formation by sonication of 4,4',4",4"'-(Pyrene-1,3,6,8-tetrayl)tetrabenzoic acid) with sodium hydroxide [1M], followed by addition of supramolecular *E*-4HPBA with help of Uv-vis spectroscopy (Fig S1). The steps are sketched in Fig. 1Di and Fig. S4. The progressive execution of the reaction with the stepwise increase of complexity shows that *E*-4HPBA plays several crucial roles in the assembly process. Firstly, it acts as crowding agent invoking depletion forces for the stacking of the Na-PyrTBA planks by forming an outer shell. This facilitates the formation of uniform rods by promoting multiphase structuring (illustration of Fig. 1Di b→c).(*40*) In fact, the multiphase structuring leads to a droplet architecture,(*41*) dictated by the relative surface tensions among the different possible interfaces (γ_{ij}) of solvent (DMF), Na-PyrTBA and *E*-4HPBA.(*16*) The relative surface tension γ_{ij} of the interfaces decreases by the formation of the outer shell of *E*-4HPBA around Na-PyrTBA, both surrounded by DMF. The shell formation further involves multivalent interactions to the similar chemically functionalized Na-PyrTBA.(*42*) It minimizes the free energy of the system as required for minimizing energetically expensive interfaces as shown in the illustration of Fig. 1Dii, which finally determines the multiphase structure. As a result, the surrounding *E*-4HPBA facilitates the growth of thicker rods comprised of a bundle of thinner rods (illustration of Fig. 1Di c→d).(*40*) Finally, *E*-4HPBA enables the thinner rods to split into a bundle of planks and thereby spread like a hand fan (or the plumes of peacocks) to form the bouquet-type structure of 1a. The spreading of planks is also found in natural materials, such as in spherulites.(*43*) This final step is brought about by the capillary action because of the Marangoni effect (or thermocapillary effect) coupled with the interfacial tension gradient between Na-PyrTBA and *E*-4HPBA as illustrated in Fig. 1Diii.(*44*) The Marangoni effect describes the change in surface tension of a liquid as a function of temperature.(*45*) The fluctuation in surface tension triggers convective movement within the fluid. The resulting motion subsequently induces the liquid to flow throughout the bulk towards the air-liquid interface. The resulting capillary force between the assembled planks in the thicker rod structure and the liquid results in their spreading to form the bouquet-type structures we observe. These actions collectively indicate a multiphase structure relationship between 1a and *E*-4HPBA. In fact, besides the bouquets of 1a, the reaction mixture contains also thinner and thicker rods (Fig. S4), which are suppressed in the favor of the bouquet formation of 1a as the reaction proceeds. As a counter experiment, we implemented photoisomers without hydroxy end group (i.e., 4-(phenylazo)benzoic acid) and additionally performed the reaction in the absence of the photoisomers. In both cases non-uniform rod-like structures formed (Fig. 1Bviii and Fig. S9), highlighting the importance of multivalent interactions of supramolecular photoisomers and the resultant difference in surface tensions

(brought only by interactions at supramolecular level) in the assembly process of the superstructures.

Twisters, 1b, are formed when *Z*-4HPBA is used *in lieu* of *E*-4HPBA (1b, Fig. 1Biii & iv). *Z*-4HPBA is formed by previous isomerization of *E*-4HPBA with UV light (λ = 254 nm) and its subsequent addition to the reaction mixture. Here, 1b is the exclusive product and consists of branches, which themselves constitute of twisted rods. These rods themselves consist of uniformly twisted planks in the form of helices. The average pitch of these helices is 3.88 µm. Each twisted plank in a branch of 1b has the same handedness, resulting in overall extrinsic chirality of the superstructure, whereas among the different superstructures different handedness is found. Notably, in this experiment, we have successfully shown the evolution of global chirality from achiral monomers. The evolution of global chirality can be elucidated by multivalent interactions of *Z*-4HPBA forming outer shell of Na-PyrTBA. Twisters inherit the shape of the preformed helical shaped *Z*-4HPBA. We conducted steady-state and time-resolved µ-Photoluminescence (µ-PL) studies on 1a and 1b to illustrate morphology-dependent emergent properties (Fig. S11). We find that the µ-PL spectrum of 1b is broadened and red shifted compared to that of 1a with maximum peaks at 2.81 eV and 2.4 eV. The red shift can be attributed to the twisted and aggregated nature of 1b. The twists scaffold induces the formation of excited state complexes (heterodimers in excited state).(*46*, *47*) These complexes show emission in higher wavelength regions (510-550 nm). The formation of the complexes in 1b indicate larger π- π overlap compared to that in 1a. (*47*, *48*) In time resolved µ-PL, we observe a faster PL decay in the 1a structure (τ = 1.06 ns) with respect to the Twisters 1b (τ = 1.41 ns). The red shift of the emission and longer PL decay time of the 1b than that of 1a ascertain the formation of excited state complexes upon photoexcitation in 1b, due to its relative twisted nature. These results highlight the specific functionality (in the form of the interaction with light) that has been transmitted to each superstructure, which is inter-distinguishable and hence, unique for the specific structure.

As a final reaction, we implemented *E*-2HPBA as supramolecular photoisomer, which forms a planar supramolecule when assembled with sodium hydroxide [1M]. The superstructure we obtained from this reaction displays flat bouquets (1c, Fig. 1Bv & vi). Such structures are formed lying beneath an extended planar network of *E*-2HPBA, which itself covers the air-liquid interface (see Fig. S12). *E*-2HPBA layers enable the horizontal action of the Marangoni effect at the surface instead of the vertical action enabled by *E/Z*-4HPBA (i.e., superstructures 1a and 1b). In fact, the average length of the planks forming 1a and 1b are similar and around 25 µm, while the average size of a plank forming 1c is 5 µm (Fig. S8). This emphasizes that linear chain supramolecules (*i.e.*, *E*-4HPBA and *Z*-4HPBA) bring forth uniform and bigger superstructures formed in vertical direction, whereas the planar supramolecule (*i.e.*, *E*-2HPBA) generates smaller superstructures, which grow parallel to the air-liquid interface. Thus far, we show supramolecular photoisomers control the pathway complexity of the solvothermal reaction of Na-PyrTBA resulting into superstructures 1a, 1b and 1c.(*49*) In this instance, we aimed to investigate the role of Zr salt in the solvothermal reaction. We conducted two experiments: first, using twice the amount of Zr compared to what was used in 1a, and second, carrying out the same reaction without any Zr salt. The experiments result into stitched bouquets (1d, Fig. 1Bvii) and rods (Fig. S13), respectively. Stitching of rods in 1d might indicate partial replacement of Na by Zr at metal-organic bonding sites of the single planks of the superstructure. The formation of rods in the absence of Zr salt instead illustrates its role on the formation of the head of the vertical bouquets of 1a and 1b. In fact, we performed elemental mapping at the base of 1a (Fig. S10), however, no trace of Zr was found. Overall, we conclude that at this concentration, Zr is not detectable in 1a, however, its presence at the air-liquid interface is essential for the formation of the uniform vertical bouquet superstructures.

Post Synthetic Response of Bouquet Superstructures in dispersions

In this section, we demonstrate the response of the superstructures to external stimuli, such as varying wavelengths of light. The superstructures of 1a are exposed to UV light (λ = 254 nm), as *E*-4HPBA forming the outer shell around 1a is supposed to transform to its *Z*-form (and take a

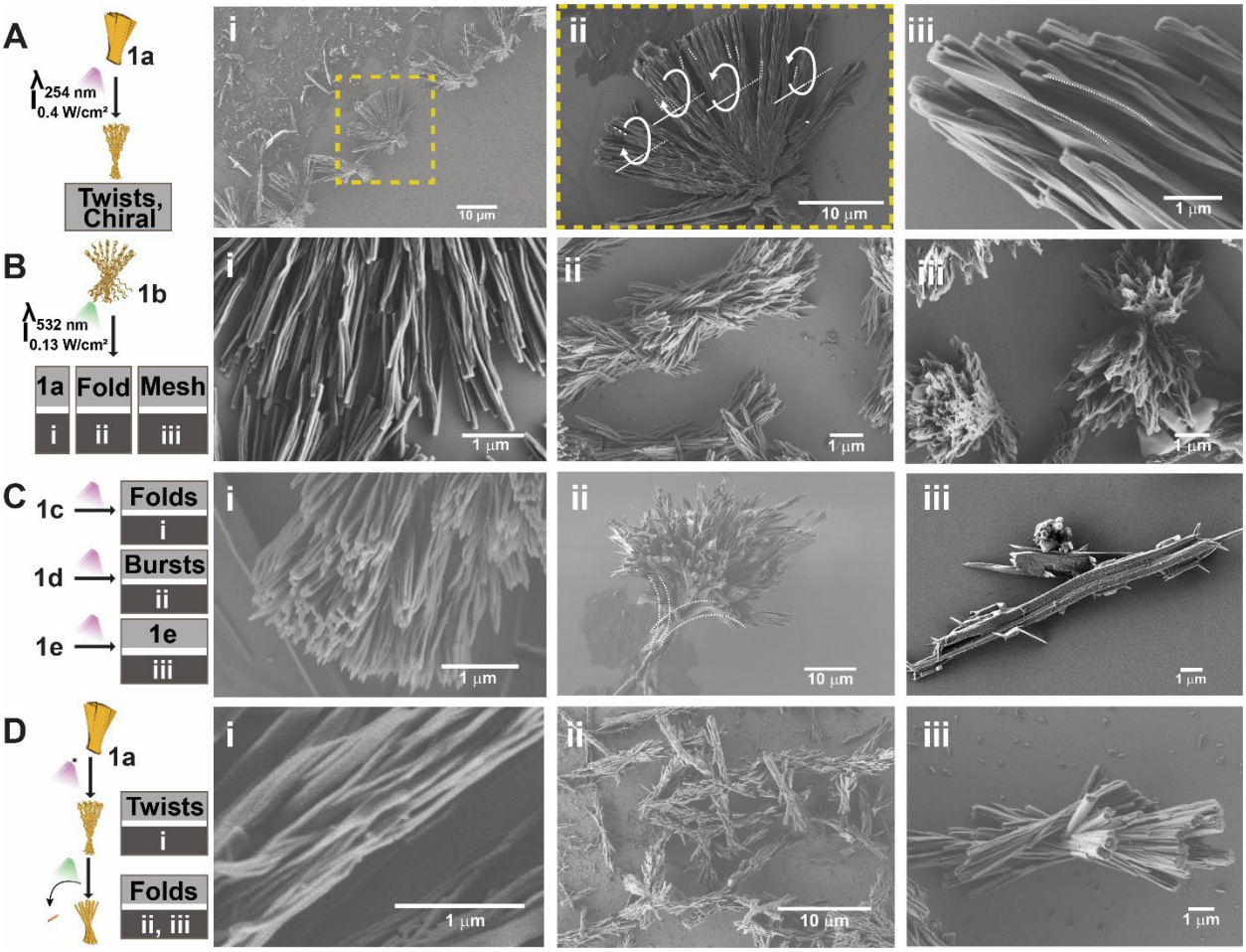

Fig. 2. Coherent Responsiveness of Bouquet Superstructures. (**A**) SEM images (i), (ii) and (iii) show coherent twists & localized chirality appearing to 1a after UV light exposure; (**B**) SEM images (i), (ii) and (iii) show structure like 1a, folds and mesh, respectively appearing to 1b after exposure to green laser. (**C**) SEM images (i), (ii), (iii) show folds and closure, bursts, and no twisting to 1c, 1d, 1e, respectively. (**D**) SEM image i. shows twists appearing in 1a. SEM images (ii) and (iii) depict folds when 1a is sequentially exposed to UV light and followed with green laser.

helical shape) upon exposure to UV light. As a result of the exposure to UV light, we observe the introduction of global chirality into the bouquet-superstructure induced by the collective twisting action of *E*-4HPBA to transform into *Z*- 4HPBA. The individual planks of 1a exhibit photomechanical response by aggregating into branches and the appearance of coherent twists. Each plank of 1a in a branch has the same handedness, i.e., induced chirality, displaying the formation of chirality from achiral monomers. The overall handedness in 1a is mixed (Fig. 2Aii). We do not detect fracture of individual planks with this prolonged exposure to UV light ($\lambda = 254$ nm). The average pitch of helices formed in each plank of twisted 1a is 4.27 μm. This average pitch is like the one found in the planks of 1b, suggesting that the initial supramolecular photoisomers, *i.e.*, *E*-4HPBA is the same for both cases.

Opposite to the superstructures of 1a, the superstructures of 1b are exposed to a green laser ($\lambda = 532$ nm), as *Z*-4HPBA present as guest in 1b is supposed to transform back to its *E*-form upon exposure to visible light. After photoexciting 1b, we observe three types of distinct populations. In the first population, the twisted planks have transformed into linear planks, as shown in Fig. 2Bi. In the second and third population, the planks have folded up and formed a mesh, respectively. Most probably due to the long exposure to the laser beam, the folded-up nature of the individual planks appears. This suggests

that the single chain polymers (*Z*-4HPBA) have detached from the architecture, while the mesh is formed possibly due to overexposure to the laser. As a control experiment, we left superstructures 1a and 1b undisturbed under ambient conditions in dispersion for 2 months, stored in the dark (Fig. S16a and Fig. S16b, respectively). The planks of 1a become hollow tubes whereas the Twisters of 1b straighten out over time. Interestingly, the intermediate rods transform into bisymmetrical flower morphology after two weeks (S16c). The combination of the three observations shows the kinetic product over time has changed due to the ongoing Marangoni effect and perhaps removal of the outer shell of the supramolecular photoisomers. The superstructures of 1c are exposed to UV light (λ = 254 nm), as the *E*-*2*HPBA is supposed to transform to its *Z*-form upon exposure to UV light. The photomechanical response after exposure to UV light results in the folding up of the individual planks of 1c, as shown in Fig. 2Ci. The folding action of individual planks can be understood as the planar *E*-2HPBA drastically aggregates when *Z*-2HPBA is formed (Fig. S1ii). The aggregated *Z*-2HPBA relinquishes to act as the external support to 1c with the consequence of folding of planks present in 1c. In another experiment, photoexciting the stitched bouquets of 1d, their bursting is observed (Fig. 2Cii). The photoexcitation induces the isomerization of *E*-4HPBA to *Z*-4HPBA embedding 1d. The stitched nature of 1d prevents *E*-4HPBA from twisting. However, the isomerization induces strong photomechanical response causing the entire superstructure to rupture. This action supports the guest nature of *E*-4HPBA inside the superstructure of 1d. Very interestingly, the coherent responsiveness of 1c and 1d mimic natural phenomena, such as the folding of the leaves of *mimosa pudica* and the bursting of seedpods, respectively.(*50*, *51*) Finally, Fig. 2Ciii depicts that 1e formed by photoisomer without the hydroxy group cannot twist the rods even after long exposure to UV light. These results illustrate the importance of the head of the bouquet-type structures of 1a and 1b, formed at the presence of Zr salt, in exhibiting the observed global chirality, where the collective twisting action of outer shell *E*-4HPBA dictates the handedness of each individual plank in a branch. In the final step, the 1a superstructure is sequentially exposed to UV light (λ = 254 nm) and a green laser (λ = 532 nm). This experiment is performed to understand the nature of successive responsiveness. The planks of 1a get twisted (Fig. 2Di) after UV exposure, as already illustrated above. Thereafter, these twisted planks get coherently folded up after exposure to green laser (Fig. 2Dii and Fig. 2Diii). Overall, the folding-up action as photo-mechanical response is observed in the following events: i) green laser exposure to 1b; ii) UV light exposure to 1c, and iii) sequential exposure of UV light and green laser to 1a. Thereby we can deduce that the folding-up action resulted due to removal of outer shell photoisomers around superstructures.

Level 2: Formation of Flower Superstructures in Droplets and Bouquet Superstructures of Matrices

In the following, we will display the execution of parallel reactions, which lead to two different well-distinguishable superstructures obtained from a one-pot reaction by exploiting LLPS and relative interfacial tension gradient. We succeeded in this endeavor by enhancing the complexity of our reaction mixture, with the purpose of inducing LLPS (similar to droplets of oil in water).(*36*) We added porphyrin (i.e., 4,4′,4″,4‴-(Porphine-5,10,15,20-tetrayl)tetrakis(benzoic acid, PorTBA) in addition to PyrTBA (3:1 PyrTBA:PorTBA, molar ratio). Porphyrin based MOFs and COFs have been studied extensively in the past for their biomedical and catalysis applications.(*52*, *53*) Hence, the new solvothermal reaction contains a mixture of Na-PyrTBA and Na-PorTBA in the presence of the supramolecular photoisomers as well as Zr salt as depicted in Fig. 3A and the progress of the reaction is illustrated in Fig S17. Both PyrTBA and PorTBA have the same denticity, however they are compositionally and conformationally different. They do not react with each other. The diluted solution of Na-PorTBA with the concentrated and less miscible dispersion of Na-PyrTBA leads to LLPS,(*36*) where PyrTBA layers form the droplet phase and Na-PorTBA form the matrix phase (Fig. 3Di). LLPS formation is a result of increased homotypic interaction and subsequent decreased heterotypic interactions at this molar concentration of Na-PyrTBA to Na-PorTBA upon prolonged sonication.(*54*) However, due to similar chemical functionalities, Na-PorTBA

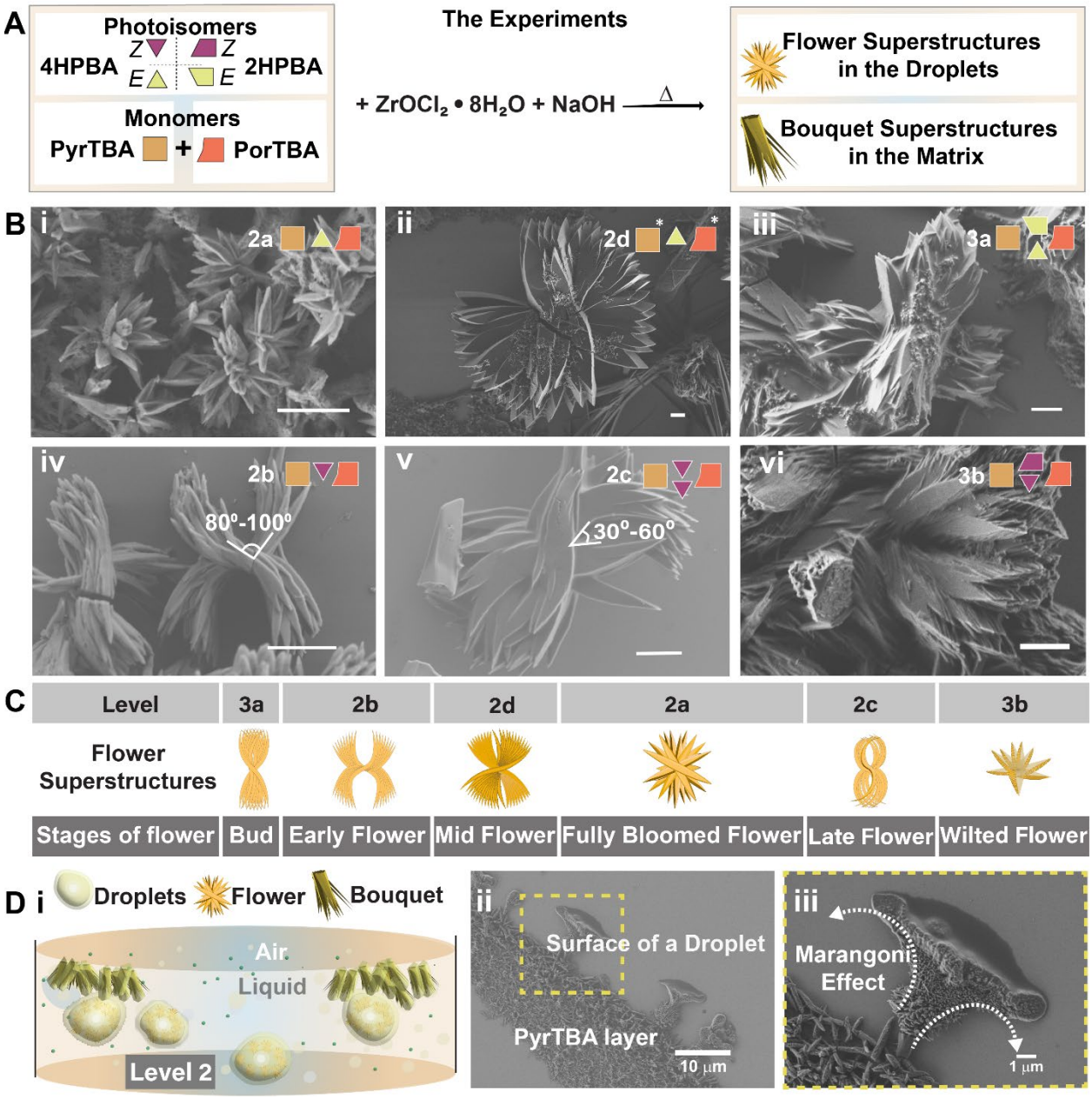

Fig. 3. Formation of Flower Superstructures in the Droplets. (**A**) Illustration of the solvothermal reaction of PyrTBA and PorTBA together with various photoisomers, resulting into a set of flower and bouquet superstructures concomitantly. (**B**) (i-vi) SEM images of a set of flower superstructures under various conditions. Scale bar = 1 μm. (**C**) Schematic illustration of the flower superstructures in (B) into different stages of a flower. (**D**) (i) Illustration depicting simultaneous reactions in droplets and in matrix. The flower superstructures are formed in droplets whereas bouquet superstructures are formed in the matrix in a segregated manner. SEM image (ii) and (iii) captures Marangoni effect at liquid-liquid interface of a droplet and the matrix.

(like Na-PyrTBA) can interact with photoisomeric supramolecules. Once the *E*-4HPBA is introduced (after the formation of droplets in matrix), i t forms the outer shell not only over the droplets to minimize the surface tension, but also induces the formation of rods embedded in *E*-4HPBA in the matrix phase. This formation of outer shell can be explained by the relative surface tension between the solvent (DMF), *E*-4HPBA and PorTBA. These two types of coated-droplets of Na-PyrTBA and Na-PorTBA avoid contact as the relative surface

tension between the two droplets is costly (high $\gamma_{34,}$ Fig. S17).(*16*) Thus, upon solvothermal reactions, two different sets of superstructures are formed concomitantly in the droplet and matrix phase, resembling flower- and bouquet-type superstructures, respectively (depicted in Fig. 3 and Fig. 4). The flower superstructures of Fig. 3 are bisymmetrical and, depending on the photoisomer and the specific concentrations used, result into a set of superstructures, which we rearranged in Fig. 3B (SEM) and Fig. 3C (sketch) to resemble the stages of a flower: the bud (3a), the early flower (2b), the mid-flower (2d), the fully bloomed flower (2a), the late flower (2c), and the wilted flower (3b). There is a distinct difference between the use of *E*- and *Z*- based supramolecular photoisomers. The flower superstructures originated from *E*- based photoisomers have similar lengths (*i.e.*, 2a and 2b) and form linear petals (*i.e.*, 2a, 2d, 3a), while *Z*- based photoisomers bring forth curved petals (*i.e.*, 2b, 2c, 3b) with lengths in the same range (Fig. S18). Upon analysis of the SEM images of 2b and 2c (Fig 3Biv and Fig. 3Bv), we notice that the central angles (marked in the figures) of the curved petal superstructures are at approximately right angles and acute angles, respectively. Hence, we deduce that upon doubling the amount of *Z*-4HPBA in the reaction mixture we can enclose almost twofold the curved petals. Interestingly, the net pattern for 2c is lemniscate, a curve shape like a figure eight or symbol of infinity.(*55*) The crystal structure of 2a and 2b confirms that both are composed of MOF of Na-PyrTBA (Fig. S3), belonging to the same crystal system as that of 1a.

In addition to the flowers, bouquet-type superstructures are formed in parallel as a result of the same solvothermal reaction (Fig. 4A). Each level of bouquet superstructures (Fig. 4A, 2a-d, 3a-b) is the result of a parallel processed reaction corresponding to the same flower superstructures (2a-d and 3a-b) shown in Fig. 3A. All bouquet superstructures have rods as base units unlike planks in Level 1. A few bouquet superstructures in 2a contain solid rods (shown by dotted arrows in Fig. 4Ai), whereas the rods of 2b are hollow (indicated by dotted arrows in Fig. 4Aii). Here, the constituent rods are not twisted unlike the planks in 1b. Moreover, the reaction performed with increased amount of photoisomers (*E*-4HBPA) does not result in bouquet formation (Fig. 4Aiii), which shows that the increased amount of photoisomers (*E*-4HBPA) in the solvothermal reaction inhibits the formation of superstructures by saturating the bonds.

Two Marangoni effects coupled with interfacial tension gradients are controlling two reactions concomitantly, one at the air-liquid interface and another at the liquid-liquid interface (between the matrix and the droplets) facilitate the occurrence of parallel reactions. Na-PyrTBA based motifs, i.e., flower superstructures and the Na-PorTBA based motifs, i.e., bouquet superstructures are formed in segregation in the droplet and the matrix phase, respectively. In Fig. 3Dii, we present a snapshot of part of the droplet displaying the Marangoni effect at the interface between the droplet and the matrix with Na-PyrTBA assemblies accumulated along the edge of the droplet. This snapshot was obtained by rapidly cooling the reaction mixture after the solvothermal reaction.

The concurrent formation of various pairs of flower and bouquet superstructures suggests that the supramolecular photoisomers collectively play a synergistic and cooperative role in generating a diverse array of morphologies. The photoisomers are present in the matrix phase rather than in the droplet phase because of the high concentration of Na-PyrTBA and relative surface tension(γ_{ij}) of solvent (DMF), Na-PyrTBA and *E*-4HBPA, which inhibits its penetration.(*41, 56*) In fact, the length of curvature in the curved flower superstructures (2b, 2c, 3b in Fig. 3B) is smaller than a pitch of the twisted bouquets (Fig. 1Ciii and Fig. 2Aii). This indicates that the photoisomers (*i.e.*, the *Z*-isomers) are present at the liquid-liquid interphase but can only partially penetrate the droplets. In this way, the photoisomers coordinate the internal droplet organization as well as the matrix organization. These photoisomers enable formation of kinetically trapped states of monomer mixtures, as discussed above, by influencing the interplay of homotypic interactions (*i.e.*, within one phase) vs. heterotypic interactions (*i.e.*, at the droplet-matrix interface). Revisiting the formation of flower superstructures observed by reducing cooling time of the reaction by half, we show an intermediary state where the petals of the flower are being carved out (Fig. 4Bi).

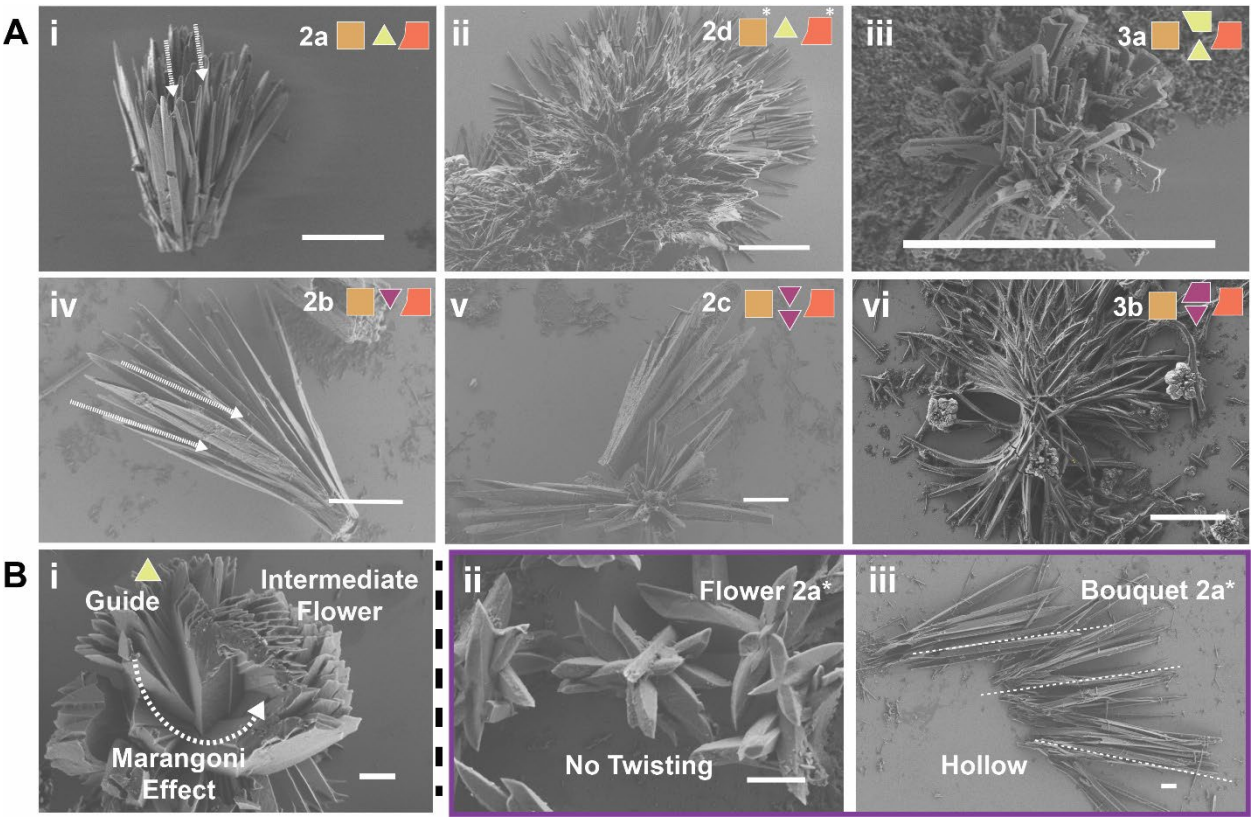

Fig. 4. Evolution of Bouquet Superstructures in the Matrices. (**A**) (i-vi) SEM images of set of bouquet superstructures formed in the matrix under various conditions. Scale bar = 10 µm. (**B**) (i) SEM image capturing the capillary action brought by supramolecular photoisomers, which facilitates the Marangoni effect; (ii) SEM image depicting the effect of UV light exposure to the superstructure 2a; (iii) SEM image illustrating the effect of UV light exposure to the rods in 2a. Scale bar = 2 µm.

Finally, the phase separated ensemble of flower and bouquet superstructures (2a) are exposed to UV light to extract information to their responsiveness. As shown in Fig 4Bii, the flower superstructure (2a, Fig. 3Bi) does not twist, which ascertains that *E*-4HBPA forming an outer layer surrounding droplets and not individual superstructures in the formation the flower superstructures. The bouquet superstructure (2a Fig. 4Ai) becomes hollow after UV exposure (as shown by dotted line in Fig. 4Biii). UV exposure isomerises *E*-4HBPA, which in turn bursts the inner core of the bouquet making the rods, which form the superstructure hollow. This confirms that individual bouquet superstructure is embedded within *E*-4HBPA. The entire system operates akin to an adaptive system with the capability to capture global-level dynamics.(*57*)

Discussion

We have developed a new synthesis approach in dispersions to form superstructures of extended molecular frameworks of sodium coordinated organic molecules able to exhibit polymorphism as shown in Level 1. Supramolecular photoisomers dictate the reaction dynamics of the superstructures formed by a bigger supramolecular monomer (*i.e.*, Na-PyrTBA) and generate kinetically trapped species with different morphologies. The involved supramolecules are formed through transitions from liquid phase to solid phase. The overall morphological development can be assigned to a combination of different physical forces working in tandem. First, the chemical mixture undergoes multiphase structuring to minimize the free energy of energetically expensive interfaces dictated by the relative surface tensions among the participating interfaces (γ_{ij}) of solvent, supramolecular monomer and supramolecular photoisomer. The participation of the supramolecular photoisomers further involves multivalent interactions to the similar chemically functionalized Na-PyrTBA. Finally, the capillary

action of the Marangoni effect (or thermocapillary effect) coupled with the interfacial tension gradient between Na-PyrTBA and the photoisomers results in their further morphological development. These actions collectively result in the formation of superstructures, while the photoisomeric supramolecules bring forth the polymorphism, featuring curved surfaces and extrinsic chirality. Coherent responsiveness of the superstructures with light as trigger was obtained by exploiting the photomechanical response of the azobenzene based photoisomeric superstructures. As a result of the multiphase structuring, transformations ranging from induced chirality to bursting and folding behaviors were observed. Notably, chirality has also been obtained from achiral superstructures upon exposure to light. While chirality is naturally inherent, synthetic chemistry frequently necessitates the utilization of chiral subunits to achieve chiral structures.(*58*) Here, we have successfully shown that macroscale chirality from achiral monomers can be achieved at the global level. It will be interesting to use these chiral environments to synthesize chiral molecules at the absence of any chiral subunit.(*59*) Time-dependent processes inducing rotational (torsional) forces are another exciting direction to target for regulated motion of these superstructures. In fact, we also demonstrate folding and bursting action induced by a simple trigger with light. These functional structure designs can further be utilized in the fields of soft robotics and drug delivery by enabling adaptability and sensibility to the environment.(*60*) Thus, we demonstrate that utilizing supramolecular photoisomers instead of individual photoisomers offers the advantage of transferring the functionality of the supramolecular photoisomer to the entire scaffold of superstructures.

At Level 2, we capitalized on the LLPS resulting from the de-mixing of two distinct multidentate monomers in a dispersion. These monomers possess identical charge and denticity, yet they differ in conformation and composition. It is also associated with their varying concentrations and compatibility with the solvent. Therefore, we have found a straightforward approach to induce LLPS by combining two small molecules. This method can serve as a model for understanding the universal, complex nature of LLPS at the cellular level. The presence of supramolecular photoisomers drives assembly of structures far richer when the complexity or crowding is enhanced. Crystalline assemblies such, as flower and bouquet structures are formed within droplets and matrix environments independently and in parallel, each exhibiting polymorphism as a result of the chosen supramolecular photoisomer. The reactions are confined within droplets, allowing the formation of intricate yet controlled curved superstructures. We comprehend the establishment of order of the flower superstructures at the droplet-matrix interface primarily because of the collective effort of chemical information, thermal energy, and mechanical energy. The provision of chemical information through photoisomers, which govern the physical properties of interfaces, is likely to play a role in shaping the dynamic superstructures through channelling capillary forces. Thermal energy facilitates the formation of superstructures within droplets by melting PyrTBA initially and the thermal gradient also originates the Marangoni effect. The mechanical energy is generated at the liquid-liquid interphase due an interfacial tension gradient.(*44*) Overall, these forces bring forth order in an unprecedented manner at the expense of exothermic heat similar to the generation of order in life. Further investigation is needed to decipher the directing mechanisms by which supramolecules (with or without metal salts) mimic molecular phase behaviour, achieve homochirality coordinate the assembly of structures resembling various physiological forms, and model pathological transformations. This brings us closer to the development of a synthetic model for intracellular phase transitions, which could serve as a foundation for the spatiotemporal organization of mimicking cellular architecture.(*11*) Complexity in Level 2 is designed to function like an adaptive system, possessing the ability to capture dynamics at the global level. Treating these results as a foundation, we are designing experiments that use light as trigger to form structures that are even more complex with multifunctional properties envisioned for far-from-equilibria regimes. Finally, we have demonstrated that controlled interactions among small molecules, defined by synthetic superstructures, can serve as a tool for

investigating complex issues pertaining to the origin of life.

References

1. G. M. Whitesides, B. Grzybowski, Self-Assembly at All Scales. *Science (1979)* **295**, 2418–2421 (2002).
2. M. Birnbaumer, Minireview: Mutations and Diseases of G Protein Coupled Receptors. *Journal of Receptors and Signal Transduction* **15**, 131–160 (1995).
3. L. Cronin, S. I. Walker, Beyond prebiotic chemistry. *Science (1979)* **352**, 1174–1175 (2016).
4. M. M. Safont-Sempere, G. Fernández, F. Würthner, Self-Sorting Phenomena in Complex Supramolecular Systems. *Chem Rev* **111**, 5784–5814 (2011).
5. J. Wang, K. Liu, R. Xing, X. Yan, Peptide self-assembly: thermodynamics and kinetics. *Chem Soc Rev* **45**, 5589–5604 (2016).
6. H. Furukawa, K. E. Cordova, M. O'Keeffe, O. M. Yaghi, The Chemistry and Applications of Metal-Organic Frameworks. *Science (1979)* **341**, 1230444 (2013).
7. J. F. Stoddart, Thither supramolecular chemistry? *Nat Chem* **1**, 14–15 (2009).
8. T. Aida, E. W. Meijer, S. I. Stupp, Functional Supramolecular Polymers. *Science (1979)* **335**, 813–817 (2012).
9. S. C. Weber, C. P. Brangwynne, Getting RNA and Protein in Phase. *Cell* **149**, 1188–1191 (2012).
10. G. Ashkenasy, T. M. Hermans, S. Otto, A. F. Taylor, Systems chemistry. *Chem Soc Rev* **46**, 2543–2554 (2017).
11. J. R. Nitschke, Molecular networks come of age. *Nature* **462**, 736–738 (2009).
12. L. Duso, C. Zechner, Stochastic reaction networks in dynamic compartment populations. *Proceedings of the National Academy of Sciences* **117**, 22674–22683 (2020).
13. A. Klosin, F. Oltsch, T. Harmon, A. Honigmann, F. Jülicher, A. A. Hyman, C. Zechner, Phase separation provides a mechanism to reduce noise in cells. *Science (1979)* **367**, 464–468 (2020).
14. T. Pederson, The Nucleolus. *Cold Spring Harb Perspect Biol* **3**, a000638 (2011).
15. J. G. Gall, The centennial of the Cajal body. *Nat Rev Mol Cell Biol* **4**, 975–980 (2003).
16. Y. Shin, C. P. Brangwynne, Liquid phase condensation in cell physiology and disease. *Science (1979)* **357**, eaaf4382 (2017).
17. I. A. Antifeeva, A. V Fonin, A. S. Fefilova, O. V Stepanenko, O. I. Povarova, S. A. Silonov, I. M. Kuznetsova, V. N. Uversky, K. K. Turoverov, Liquid–liquid phase separation as an organizing principle of intracellular space: overview of the evolution of the cell compartmentalization concept. *Cellular and Molecular Life Sciences* **79**, 251 (2022).
18. C. P. Brangwynne, P. Tompa, R. V. Pappu, Polymer physics of intracellular phase transitions. *Nat Phys* **11**, 899–904 (2015).
19. C.-H. Choi, D. S. W. Lee, D. W. Sanders, C. P. Brangwynne, Condensate interfaces can accelerate protein aggregation. *Biophys J*, doi: https://doi.org/10.1016/j.bpj.2023.10.009 (2023).
20. U. Rana, N. S. Wingreen, C. P. Brangwynne, A. Z. Panagiotopoulos, Interfacial exchange dynamics of biomolecular condensates are highly sensitive to client interactions. *J Chem Phys* **160**, 145102 (2024).
21. L. Shang, Y. Zhao, Droplet-Templated Synthetic Cells. *Matter* **4**, 95–115 (2021).
22. H. Fu, J. Huang, J. J. B. van der Tol, L. Su, Y. Wang, S. Dey, P. Zijlstra, G. Fytas, G. Vantomme, P. Y. W. Dankers, E. W. Meijer, Supramolecular polymers form tactoids through liquid–liquid phase separation. *Nature* **626**, 1011–1018 (2024).
23. C. Yuan, M. Yang, X. Ren, Q. Zou, X. Yan, Porphyrin/Ionic-Liquid Co-assembly Polymorphism Controlled by Liquid–Liquid Phase Separation. *Angewandte Chemie International Edition* **59**, 17456–17460 (2020).
24. C. Alfano, Y. Fichou, K. Huber, M. Weiss, E. Spruijt, S. Ebbinghaus, G. De Luca, M. A. Morando, V. Vetri, P. A.

Temussi, A. Pastore, Molecular Crowding: The History and Development of a Scientific Paradigm. *Chem Rev* **124**, 3186–3219 (2024).
25. N. Bäumer, E. Castellanos, B. Soberats, G. Fernández, Bioinspired crowding directs supramolecular polymerisation. *Nat Commun* **14**, 1084 (2023).
26. C. Yuan, A. Levin, W. Chen, R. Xing, Q. Zou, T. W. Herling, P. K. Challa, T. P. J. Knowles, X. Yan, Nucleation and Growth of Amino Acid and Peptide Supramolecular Polymers through Liquid–Liquid Phase Separation. *Angewandte Chemie International Edition* **58**, 18116–18123 (2019).
27. A. I. Hanopolskyi, T. A. Mikhnevich, A. Paikar, B. Nutkovich, I. Pinkas, T. Dadosh, B. S. Smith, N. Orekhov, E. V Skorb, S. N. Semenov, Interplay between autocatalysis and liquid-liquid phase separation produces hierarchical microcompartments. *Chem* **9**, 3666–3684 (2023).
28. F. P. Kinik, A. Ortega-Guerrero, D. Ongari, C. P. Ireland, B. Smit, Pyrene-based metal organic frameworks: from synthesis to applications. *Chem Soc Rev* **50**, 3143–3177 (2021).
29. J. Sun, H. Sekhar Jena, C. Krishnaraj, K. Singh Rawat, S. Abednatanzi, J. Chakraborty, A. Laemont, W. Liu, H. Chen, Y.-Y. Liu, K. Leus, H. Vrielinck, V. Van Speybroeck, P. Van Der Voort, Pyrene-Based Covalent Organic Frameworks for Photocatalytic Hydrogen Peroxide Production. *Angewandte Chemie International Edition* **62**, e202216719 (2023).
30. J. Miao, W. Graham, J. Liu, E. C. Hill, L.-L. Ma, S. Ullah, H.-L. Xia, F.-A. Guo, T. Thonhauser, D. M. Proserpio, J. Li, H. Wang, An Octacarboxylate-Linked Sodium Metal–Organic Framework with High Porosity. *J Am Chem Soc* **146**, 84–88 (2024).
31. F. A. Jerca, V. V. Jerca, R. Hoogenboom, Advances and opportunities in the exciting world of azobenzenes. *Nat Rev Chem* **6**, 51–69 (2022).
32. H. M. D. Bandara, S. C. Burdette, Photoisomerization in different classes of azobenzene. *Chem Soc Rev* **41**, 1809–1825 (2012).
33. M. Kondo, Photomechanical materials driven by photoisomerization or photodimerization. *Polym J* **52**, 1027–1034 (2020).
34. J. Liu, S. Wang, T. Huang, P. Manchanda, E. Abou-Hamad, S. P. Nunes, Smart covalent organic networks (CONs) with "on-off-on" light-switchable pores for molecular separation. *Sci Adv* **6**, eabb3188 (2024).
35. W. Danowski, T. van Leeuwen, W. R. Browne, B. L. Feringa, Photoresponsive porous materials. *Nanoscale Adv* **3**, 24–40 (2021).
36. L. Tang, Liquid phase separation. *Nat Methods* **16**, 18 (2019).
37. T. C. Wang, N. A. Vermeulen, I. S. Kim, A. B. F. Martinson, J. F. Stoddart, J. T. Hupp, O. K. Farha, Scalable synthesis and post-modification of a mesoporous metal-organic framework called NU-1000. *Nat Protoc* **11**, 149–162 (2016).
38. T. E. Webber, S. P. Desai, R. L. Combs, S. Bingham, C. C. Lu, R. L. Penn, Size Control of the MOF NU-1000 through Manipulation of the Modulator/Linker Competition. *Cryst Growth Des* **20**, 2965–2972 (2020).
39. M. Gemmi, E. Mugnaioli, T. E. Gorelik, U. Kolb, L. Palatinus, P. Boullay, S. Hovmöller, J. P. Abrahams, 3D Electron Diffraction: The Nanocrystallography Revolution. *ACS Cent Sci* **5**, 1315–1329 (2019).
40. F. Xiu, A. Knežević, J. Huskens, T. Kudernac, Interplay of Depletion Forces and Biomolecular Recognition in the Hierarchical Assembly of Supramolecular Tubes. *Small* **19**, 2207098 (2023).
41. S. Patra, S. Chandrabhas, S. Dhiman, S. J. George, Controlled Supramolecular Polymerization via Bioinspired, Liquid–Liquid Phase Separation of Monomers. *J Am Chem Soc* **146**, 12577–12586 (2024).
42. P. Li, S. Banjade, H.-C. Cheng, S. Kim, B. Chen, L. Guo, M. Llaguno, J. V Hollingsworth, D. S. King, S. F. Banani, P. S. Russo, Q.-X. Jiang, B. T. Nixon, M. K. Rosen, Phase transitions in the

assembly of multivalent signalling proteins. *Nature* **483**, 336–340 (2012).
43. A. G. Shtukenberg, Y. O. Punin, E. Gunn, B. Kahr, Spherulites. *Chem Rev* **112**, 1805–1838 (2012).
44. B. Gouveia, Y. Kim, J. W. Shaevitz, S. Petry, H. A. Stone, C. P. Brangwynne, Capillary forces generated by biomolecular condensates. *Nature* **609**, 255–264 (2022).
45. C. N. Baroud, "Thermocapillarity" in *Encyclopedia of Microfluidics and Nanofluidics*, D. Li, Ed. (Springer US, Boston, MA, 2013; https://doi.org/10.1007/978-3-642-27758-0_1567-4), pp. 1–7.
46. B. D. Wagner, G. J. McManus, B. Moulton, M. J. Zaworotko, Exciplex fluorescence of {[Zn(bipy)1.5(NO3)2}]·CH3OH·0.5pyrene}n: a coordination polymer containing intercalated pyrene molecules (bipy = 4,4′-bipyridine). *Chemical Communications*, 2176–2177 (2002).
47. X. Li, J. Yu, Z. Lu, J. Duan, H. C. Fry, D. J. Gosztola, K. Maindan, S. S. Rajasree, P. Deria, Photoinduced Charge Transfer with a Small Driving Force Facilitated by Exciplex-like Complex Formation in Metal–Organic Frameworks. *J Am Chem Soc* **143**, 15286–15297 (2021).
48. Y. Ge, Y. Wen, H. Liu, T. Lu, Y. Yu, X. Zhang, B. Li, S.-T. Zhang, W. Li, B. Yang, A key stacking factor for the effective formation of pyrene excimer in crystals: degree of π–π overlap. *J Mater Chem C Mater* **8**, 11830–11838 (2020).
49. E. Mattia, S. Otto, Supramolecular systems chemistry. *Nat Nanotechnol* **10**, 111–119 (2015).
50. W. S. Y. Wong, M. Li, D. R. Nisbet, V. S. J. Craig, Z. Wang, A. Tricoli, Mimosa Origami: A nanostructure-enabled directional self-organization regime of materials. *Sci Adv* **2**, e1600417 (2024).
51. H. Hofhuis, D. Moulton, T. Lessinnes, A.-L. Routier-Kierzkowska, R. J. Bomphrey, G. Mosca, H. Reinhardt, P. Sarchet, X. Gan, M. Tsiantis, Y. Ventikos, S. Walker, A. Goriely, R. Smith, A. Hay, Morphomechanical Innovation Drives Explosive Seed Dispersal. *Cell* **166**, 222–233 (2016).
52. J. Chen, Y. Zhu, S. Kaskel, Porphyrin-Based Metal–Organic Frameworks for Biomedical Applications. *Angewandte Chemie International Edition* **60**, 5010–5035 (2021).
53. G. Lin, H. Ding, R. Chen, Z. Peng, B. Wang, C. Wang, 3D Porphyrin-Based Covalent Organic Frameworks. *J Am Chem Soc* **139**, 8705–8709 (2017).
54. M. Phillips, K. Ghosh, Rules of selective condensation in cells. *Nat Chem*, doi: 10.1038/s41557-024-01525-w (2024).
55. M. Erickson, Ed., "Imaginative Words" in *Beautiful Mathematics* (Mathematical Association of America, 2011; https://www.cambridge.org/core/product/986389556E53549433F9B8F51756A51C)*Spectrum*, pp. 1–12.
56. Y. Shin, J. Berry, N. Pannucci, M. P. Haataja, J. E. Toettcher, C. P. Brangwynne, Spatiotemporal Control of Intracellular Phase Transitions Using Light-Activated optoDroplets. *Cell* **168**, 159-171.e14 (2017).
57. J.-M. Lehn, Perspectives in Chemistry—Aspects of Adaptive Chemistry and Materials. *Angewandte Chemie International Edition* **54**, 3276–3289 (2015).
58. N. H. Cho, A. Guerrero-Martínez, J. Ma, S. Bals, N. A. Kotov, L. M. Liz-Marzán, K. T. Nam, Bioinspired chiral inorganic nanomaterials. *Nature Reviews Bioengineering* **1**, 88–106 (2023).
59. B. S. Green, M. Lahav, D. Rabinovich, Asymmetric synthesis via reactions in chiral crystals. *Acc Chem Res* **12**, 191–197 (1979).
60. I. Apsite, S. Salehi, L. Ionov, Materials for Smart Soft Actuator Systems. *Chem Rev* **122**, 1349–1415 (2022).

Acknowledgments:
The authors thank Dr. Simone Lauciello (IIT Electron Microscopy Facility) for SEM-EDS analyses. IRP and YW thank the support of Research & Innovation and the Office of

Information Technology at the University of Nevada, Reno for facilitation and access to the Pronghorn High-Performance Computing Cluster. IRP and LM thank the computing resources provided by CRESCO/ENEAGRID High Performance Computing infrastructure. CRESCO/ENEAGRID High Performance Computing infrastructure is funded by ENEA, the Italian National Agency for New Technologies, Energy and Sustainable Economic Development and by Italian and European research programs (http://www.cresco.enea.it/english).

Funding:

PR, AA and IK received financial support of both the European Union's Horizon 2020 Research and Innovation program under grant agreement no. 101017821 (LIGHT-CAP FET proactive project), the European Union's Horizon 2020 European Research Council under grant agreement no. 850875 (Light-DYNAMO project), the Horizon Europe European Research Council Proof of Concept under grant agreement no. 101069295 (CONDINKS project), and the Ministero dell'Istruzione, dell'Università e della Ricerca (PRIN 2017 no. 2017KFY7XF and "Dipartimenti di Eccellenza 2018–2022" program). MDFD and MG received European Union's Horizon 2020 Research and Innovation Programme under the Marie Skłodowska-Curie grant agreement no. 956099 (NanED−Electron Nanocrystallography−H2020-MSCAITN).

Author contributions:

Conceptualization: PR, Methodology: PR, Visualization: SEM imaging, photo-spectroscopy measurements, photo-reversibility experiments, image analysis – PR, μ-PL experiments, laser assisted reversibility experiments - AA, electron diffraction to obtain crystal information- MDF and MG, the DFT calculations and theoretical analysis - IRP and LM. the theoretical mechanical properties calculations- IRP, YW, Funding acquisition: IK, Project administration: IK, Supervision: IK, Writing – original draft: PR, IK, Writing – review & editing: PR, IK, MDF, AA, IRP, LM, MG, YW, IK

Competing interests:

Authors declare that they have no competing interests.

Data and materials availability:

All data are available in the main text or the supplementary materials.

Supplementary Materials

Materials and Methods

Figs. S1 to S31

Table S1 to S3

References